Controllable spin-dependent transport in armchair graphene nanoribbon structures

V. Hung Nguyen,[1,2,a)] V. Nam Do,[3] A. Bournel,[1] V. Lien Nguyen,[2] and P. Dollfus[1]
[1]*Institut d'Electronique Fondamentale, UMR 8622, CNRS, Universite Paris Sud, 91405 Orsay, France*
[2]*Department of Theoretical, Institute of Physics, VAST, P.O. Box 429 Bo Ho, Hanoi 10000, Vietnam*
[3]*Hanoi Advanced School of Science and Technology, 40 Ta Quang Buu, Hanoi 10000, Vietnam*

(Received 15 May 2009; accepted 31 July 2009; published online 8 September 2009)

Using the nonequilibrium Green's functions formalism in a tight binding model, the spin-dependent transport in armchair graphene nanoribbons controlled by a ferromagnetic gate is investigated. Beyond the oscillatory behavior of conductance and spin polarization with respect to the barrier height, which can be tuned by the gate voltage, we especially analyze the effects of width-dependent band gap and of the nature of contacts. The oscillation of spin polarization in graphene nanoribbons with a large band gap is strong in comparison with that in infinite graphene sheets. Very high spin polarization (close to 100%) is observed in normal-conductor/graphene/normal-conductor junctions. Moreover, we find that the difference in electronic structure between normal conductor and graphene generates confined states which have a strong influence on the transport properties of the device. This study suggests that the device should be carefully designed to obtain a high controllability of spin-polarized current. © *2009 American Institute of Physics*.
[doi:10.1063/1.3212984]

I. INTRODUCTION

Graphene, a monolayer of carbon atoms packed into a two dimensional honeycomb lattice, has attracted much attention from both experimental and theoretical points of view (see the recent review[1] and references therein) since it was isolated and demonstrated to be stable.[2,3] It is a basic building block for graphite materials of all other dimensionalities, e.g., it can be wrapped up into zero-dimensional fullerenes, rolled into one-dimensional (1D) nanotubes, or stacked into three-dimensional graphite. Due to its unique electronic properties, i.e., the massless Dirac-like behavior of low-energy excitations,[3,4] a lot of interesting phenomena such as the finite conductance at zero concentration,[3] the unusual half integer quantum Hall effect,[4] and the Klein tunneling[5] have been widely observed and theoretically discussed in detail.[3,6]

When graphene is patterned into a narrow ribbon, the carriers are confined to a quasi-1D system, which is often referred to as a graphene nanoribbon (GNR). Actually, GNR is one of the most simple and fundamental fragments of the sp^2 network that has been very extensively studied due to its potential applicability.[7–12] The electronic properties of GNRs depend strongly on the shape of edges, e.g., it can be zigzag or armchair. It was shown by Fujita *et al.*[8,9] that, in the framework of the nearest neighbor tight binding (NNTB) model, the zigzag GNRs are always metallic, while the armchair ones may be either semiconducting or metallic depending on their width. In particular, zigzag GNRs exhibit a special edge state that makes the energy band almost flat near the Fermi energy $[E=0]$, and therefore the group velocity of conduction electrons becomes close to zero. The transport properties of these structures are then dominated by the edge states.[10] No such edge state appears in armchair GNRs, which are predicted having an energy band with either finite or zero gap. In general, the group velocity of conduction electrons in armchair GNRs is high, e.g., it is equal to about 10^6 m/s (Ref. 3) for metallic armchair GNRs. Note that the scanning tunneling microscopy measurements,[10,13] while clearly demonstrating the existence of edge states in zigzag GNRs, prove that, in practice, zigzag edges are much smaller in length than armchair ones and less frequently observed.[10] This observation and the fact that armchair GNRs may exhibit semiconducting behavior motivate us to study just these structures in the present work.[14]

Along with unusual charge transport properties, due to very weak spin orbit interaction,[15] leading to a long spin flip length (~ 1 μm),[16] the graphene-based structures also offer a high potential for spin-polarized electronics. In fact, graphene is not a natural ferromagnet. However, recent works have shown that ferromagnetism and spin-polarized states can be introduced in graphene, e.g., by doping or defects[17–19] and even by applying an external electric field.[20] Especially, Haugen *et al.*[21] suggested that the ferromagnetic correlations can be created in graphene by the so-called proximity effect. The exchange splitting induced by depositing a ferromagnetic insulator EuO on the graphene was then roughly estimated to be about 5 meV. Motivated by this suggestion, a possibility of controlling the spin-polarized current in graphene sheets using ferromagnetic gates has just predicted and in detail discussed in a number of works.[22–24] The spin-polarized current was found to be an oscillatory function of the potential barrier, which can be tuned by the gate voltage, and its amplitude is never damped by increasing the width as well as the height of barrier.[22] However, the spin polarization predicted is not so high, i.e., its maximum value is just about 30%. This may limit the possible applications of

[a)]Electronic mail: viet-hung.nguyen@u-psud.fr.

 © 2009 American Institute of Physics

Author complimentary copy. Redistribution subject to AIP license or copyright, see http://jap.aip.org/jap/copyright.jsp

graphene-based devices in spintronics. By the way, some other spin-dependent properties of graphene such as spin field effect transistor,[25] spin Hall effects,[15,26] and spin valve effects[27–30] are also extensively discussed. In particular, very interesting spin-transport phenomena in GNRs, e.g., the giant magnetoresistance[29,30] and the high spin-polarized current[31] (close to 100%), have been just predicted.

Experimentally, electronic transport measurements through a graphene device usually require contacts to metal electrodes, e.g., as illustrated in Ref. 32. When tunneling from metal reservoir to graphene occurs in a large area, the contact becomes Ohmic and the area under the contact forms a substance, which is a hybrid between graphene and normal metal.[33] Depending on the nature of this substance, the system can be appropriately considered as a graphene/graphene/graphene (GGG) structure or a normal-conductor/graphene/normal-conductor (NGN) junction whose contacts can be modeled by honeycomb or square lattices, respectively. The ballistic transport through the NGN junctions has been investigated systematically in Refs. 33–35.

The present work is focused on studying the electrical controllability of the spin-polarized current in single ferromagnetic gate structures based on perfect armchair GNRs. Examining device transport properties, we look for the possibilities of having a high tunable spin-polarized current. A particular attention is drawn to the role of the ribbon's energy band gap and of the nature of contacts (graphitic or normal conducting). For NGN junctions, when the strength of device-to-contact coupling and the device length are the two important parameters, the influence of these parameters on controlling the spin-polarized current is also carefully investigated. The work is organized as follows. Section II is devoted to describing the model and introducing the main expressions based on the nonequilibrium Green's function (NEGF) formalism. In Sec. III, the numerical results are presented and discussed. Finally, a brief summary is given in Sec. IV.

II. MODEL AND FORMULATION

The considered structures consist of an armchair GNR coupled with two semi-infinite leads, which may be described as either graphitic [Fig. 1(a)] or normal conducting [Fig. 1(b)]. In the simplest consideration, the normal-conducting leads are modeled by square lattices.[33–35] A ferromagnetic gate is assumed to create a potential barrier which controls the Fermi level locally and to induce an exchange splitting into the device. To model the structures, we use the single band tight binding Hamiltonian,

$$\hat{H} = \hat{H}_L + \hat{H}_D + \hat{H}_R + \hat{H}_C, \tag{1}$$

where $\hat{H}_{L,R}$ are the Hamiltonians of the left and right leads, respectively, $\hat{H}_D$ is the Hamiltonian of the device, and $\hat{H}_C$ describes the coupling of the device to the leads. The Hamiltonian terms in Eq. (1) can be written as

$$\hat{H}_\alpha = \varepsilon_\alpha \sum_{i_\alpha,\sigma} c^\dagger_{i_\alpha,\sigma} c_{i_\alpha,\sigma} - t_L \sum_{\langle i_\alpha,j_\alpha\rangle,\sigma} c^\dagger_{i_\alpha,\sigma} c_{j_\alpha,\sigma},$$

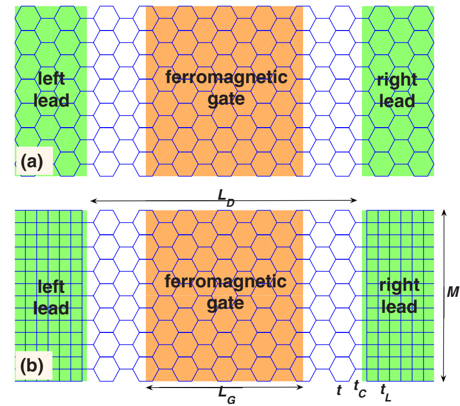

FIG. 1. (Color online) Schematic illustration of the considered armchair GNR structures with the number M of carbon chains between two edges: (a) graphitic and (b) normal-conducting leads. The latter ones are modeled by square lattices. A magnetic gated insulator is deposited to create a spin-dependent potential barrier in the center of device.

$$\hat{H}_D = \sum_{i_d,\sigma} \varepsilon_{i_d,\sigma} a^\dagger_{i_d,\sigma} a_{i_d,\sigma} - t \sum_{\langle i_d,j_d\rangle,\sigma} a^\dagger_{i_d,\sigma} a_{j_d,\sigma},$$

$$\hat{H}_C = -t_C \sum_{\alpha=\{L,R\}} \sum_{\langle i_\alpha,j_d\rangle,\sigma} (c^\dagger_{i_\alpha,\sigma} a_{i_d,\sigma} + \text{H.c.}), \tag{2}$$

where the operators $c^\dagger_{i_\alpha,\sigma}$ ($c_{i_\alpha,\sigma}$) and $a^\dagger_{i_d,\sigma}$ ($a_{i_d,\sigma}$) create (annihilate) an electron with spin σ in the electrode α and the device region, respectively; t, t_L, and t_C stand for the hopping parameters in the device, the lead, and at the coupling interface, respectively; ε_α is the on-site energy of the leads which acts as a shift in energy. The sums over carbon atoms $\langle i,j\rangle$ are restricted to the nearest neighbor atoms. The device spin-dependent on-site energy $\varepsilon_{i_d,\sigma}$ is modulated by the gate voltage,

$$\varepsilon_{i_d,\sigma} = \begin{cases} U_G - \sigma h & \text{in gated region} \\ 0 & \text{otherwise.} \end{cases} \tag{3}$$

Here, U_G denotes the potential barrier height, h is the exchange splitting, and $\sigma = \pm 1$ describes the up/down spin states.

Since there is no spin flip process here, the Hamiltonian (1) can be separated into two independent components $\hat{H}_\sigma$ and the transport can be easily considered using the NEGF formalism. For each spin channel σ, the retarded Green's function is defined as

$$\hat{G}^r_\sigma(E) = [E + i0^+ - \hat{H}_{D,\sigma} - \hat{\Sigma}^r_L - \hat{\Sigma}^r_R]^{-1}, \tag{4}$$

where $\hat{\Sigma}^r_\alpha$ describes the retarded self-energy matrices which contain the information about the electronic structure of the leads as well as the device-to-contact coupling. It can be expressed as $\hat{\Sigma}^r_\alpha = \hat{\tau}_{D,\alpha} \hat{g}_\alpha \hat{\tau}_{\alpha,D}$, where $\hat{\tau}$ is the hopping matrix that couples the device to the leads. $\hat{g}_\alpha$ are the surface Green's functions of the uncoupled leads, i.e., the left or right semi-infinite electrodes. The surface Green's functions and the device Green's functions are calculated using the fast iterative scheme[36] and the recursive algorithm,[37] respectively.

Author complimentary copy. Redistribution subject to AIP license or copyright, see http://jap.aip.org/jap/copyright.jsp

Within the model described by Eq. (1), the transport is considered ballistic and the conductance of the device can be calculated using the Landauer formalism.[38] The spin-dependent conductances $\mathcal{G}_\sigma$ at the Fermi energy E_F are related to the transmission function $T_\sigma(E)$ as

$$\mathcal{G}_\sigma(E_F) = \frac{e^2}{h} T_\sigma(E_F), \tag{5}$$

with

$$T_\sigma(E) = \mathrm{Tr}[\hat{\Gamma}_L \hat{G}^r_\sigma \hat{\Gamma}_R \hat{G}^a_\sigma]. \tag{6}$$

Here, $\hat{G}^a_\sigma(\equiv \hat{G}^{r\dagger}_\sigma)$ denotes the advanced Green's function. The tunneling rate matrix $\hat{\Gamma}_{L(R)}$ for the left (right) lead is obtained from

$$\hat{\Gamma}_{L/R} = i[\hat{\Sigma}^r_{L/R} - \hat{\Sigma}^a_{L/R}], \tag{7}$$

where $\hat{\Sigma}^a_\alpha(\equiv \hat{\Sigma}^{r\dagger}_\alpha)$ is the advanced self-energy.

Finally, the spin polarization is determined by

$$P = \frac{\mathcal{G}_\uparrow - \mathcal{G}_\downarrow}{\mathcal{G}_\uparrow + \mathcal{G}_\downarrow}. \tag{8}$$

In addition, the local density of states (LDOS) at site j can be also directly extracted from the retarded Green's function:

$$\mathrm{LDOS}_{(j)} = -\frac{1}{\pi} \mathrm{Im}\, G^r(j,j). \tag{9}$$

By using the recursive algorithm described in Ref. 37, the size of the matrices above equals the number M of carbon chains between two edges and therefore the cost of calculations is only linearly dependent on the device length.

III. RESULTS AND DISCUSSION

Within the framework of the formalism described, we investigate the spin-dependent transport in armchair GNRs with different structure parameters. The hopping parameter t is chosen to be 2.66 eV (Ref. 39) in the graphitic regions and the study is restricted to the low-energy regime when $E \ll t$.

A. Gate-controlled spin-polarized current in GGG structures

As mentioned above, the gate voltage creates a potential barrier in the device. In the armchair GNRs, the electronic properties of the structures with $M \neq 3n+2$ and $M = 3n+2$ (n is an integer) are significantly different, i.e., there is a finite energy band gap in the former structures ("semiconducting") while it is negligible in the latter ones ("metallic").[11] Respectively, we display in Fig. 2(a) the conductance as a function of barrier height U_G for the structures: semiconducting ($M=21$, dashed line) and metallic ($M=23$, solid line). Here, the gated region is assumed to be nonmagnetic, i.e., $h=0$ meV. First, the obtained results show oscillatory behaviors of conductance with respect to U_G. This phenomenon has been observed in graphene sheets and explained as a consequence of well-known Klein's tunneling.[6,22] In the framework of Dirac's description, the conductance peaks have been demonstrated to be essentially due to the resonance or the good

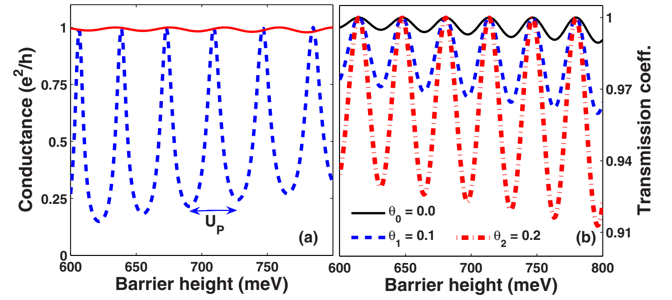

FIG. 2. (Color online) (a) Oscillation of conductance vs the barrier height U_G in the GGG structures with different widths: $M=21$ (semiconducting, dashed) and 23 (metallic, solid line). (b) illustrates the transmission coefficient calculated from Eq. (10) for different modes θ_j. Other parameters are $L_G=42.5$ nm, $E_F=300$ meV, and $h=0$ meV.

matching of electron states and confined hole states outside/inside the barrier region,[23] respectively. These states, in the model considered, correspond to states in positive and negative energy bands. Note that due to the finite ribbon width, the transverse momentum is quantized into a set of discrete values. Practically, the oscillation of conductance can be seen clearly from the expression of the transmission coefficient for a given transverse momentum mode k^j_y (see the calculation in Ref. 40). In the limit of low energy, it can be rewritten as

$$T = \frac{\cos^2\theta_j \sin^2\phi}{\cos^2\theta_j \sin^2\phi + (\sin\theta_j + \cos\phi)^2 \sin^2(k^b_x L_G)}, \tag{10}$$

where $\theta_j = \tan^{-1}(k^j_y/k_x)$ and $\sin\phi = [(t - v_F k^j_y)\sin(3ak^b_x/2)]/(U_G - E)$ with $v_F = 3at/2$, and a being the C–C bond length; $k_x(k^j_y)$ denotes the longitudinal (transverse) momentum, which is the deviation of the momentum $\vec{k}$ from the zero energy point, outside the barrier; k^b_x is the longitudinal momentum inside the barrier. The energy dispersions outside/inside the barrier are, respectively,

$$E = v_F\sqrt{k^2_x + k^{j2}_y} \tag{11}$$

and

$$U_G - E = \sqrt{4t(t - v_F k^j_y)\sin^2\frac{3ak^b_x}{4} + v^2_F k^{j2}_y}, \tag{12}$$

with $E < U_G$. Accordingly, the transmission and then the conductance have their maximum (or minimum) values when $k^b_x L_G$ is equal to $m\pi$ [or $(m+1/2)\pi$] with m being an integer. In the limit of $E \ll U_G \ll t$, Eq. (12) can be rewritten as $U_G - E \approx v_F k^b_x$ and the period of oscillation is defined by $U_P = v_F \pi / L_G$, which coincides with that in Refs. 22 and 23. In the case when the relation between U_G and $\vec{k}$ is nonlinear, this period can be approximately expressed as $U_P = v_g \pi / L_G$, in which $v_g \leq v_F$ and decreases gradually with increasing U_G. For instance, $v_g \approx 0.74 v_F (M=21)$ and $0.89 v_F (M=23)$ in the energy range considered in Fig. 2(a).

As a consequence of the difference in band structure, Fig. 2(a) also shows that the conductance in the case of $M=21$ (finite band gap) oscillates strongly in comparison with the case of $M=23$ (negligible band gap). This can be easily understood by considering the behavior of transmission coefficient for different band gaps, $E^j_g = 2v_F|k^j_y|$ [or $2E_F|\sin\theta_j|$

Author complimentary copy. Redistribution subject to AIP license or copyright, see http://jap.aip.org/jap/copyright.jsp

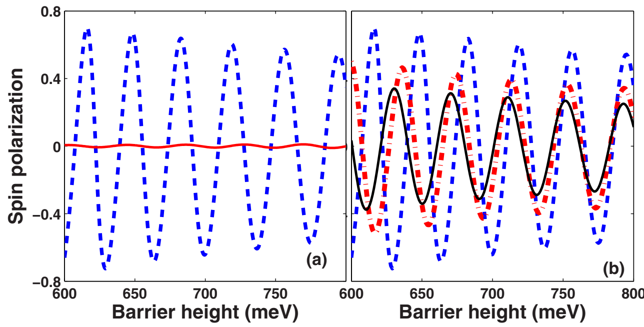

FIG. 3. (Color online) (a) Spin polarization as a function of the barrier height U_G for the same structures as in Fig. 2(a). (b) shows an example of the effects of the different ribbon widths on the spin polarization: $M=21$ (dashed), 27 (dashed-dotted), and 33 (solid line). Everywhere $L_G=42.5$ nm, $E_F=300$ meV, and $h=10$ meV.

with $\theta_j \in (-\pi/2, \pi/2)$]. They are enlarged when increasing $|k_y^j|$ (or $|\theta_j|$). Practically, when the band gap is larger, the oscillation of transmission is stronger [see in Eq. (10) and Fig. 2(b)]. This leads to the different behaviors of conductance, as shown in Fig. 2(a). Similarly, the oscillation of conductance in the structure with $M=21$ is also stronger than that in graphene sheets [see in Fig. 2(a) of Ref. 22], where the gap is truly zero.

In Eqs. (10)–(12), the mode $\theta_0=0$ (or $k_y^0=0$) corresponds essentially to the normal incident mode whose energy dispersion is gapless and linear in infinite graphene sheets. When considering the behavior of transmission coefficient, we find an important feature: it is not uniformly equal to unity but a function of the barrier height even in the case of $\theta=\theta_0$. This differs from the prediction of Klein's paradox observed in graphene sheets by using the Dirac's description[6] as previously discussed in Ref. 41. In reality, the transmission coefficient [Eq. (10)] approaches the simplified expression (4) in Ref. 6 only in the limit of $E \ll U_G \ll t$.

Now we investigate the behavior of spin-polarized current in the ferromagnetic gate structures. The exchange splitting h is chosen to be 10 meV, which can be achieved experimentally.[16,42] Since no spin flip process is considered, the exchange splitting just shifts the conductance of each spin channel relatively to the other. Therefore, the spin polarization behaves as an oscillatory function of U_G, as shown in Fig. 3. Similar phenomena in graphene sheets have been observed and discussed in Refs. 22–24. It was shown that the oscillation of spin-polarized current is never damped by increasing the width and the height of barrier. Thus, the spin polarization can be reversed by changing the gate voltage. Actually, the amplitude of P depends principally on the phase coherence/decoherence of the oscillations of spin-dependent conductance, i.e., it has the maximum/minimum value when the gate length (or the barrier width) L_G is equal to a half-integer/integer of L_h with $L_h=v_g\pi/2h$, respectively. Hence, the gate control of spin-polarized current can be modulated by changing L_G, i.e., it leads to the beating behavior of P similar to that shown in Fig. 5(c) of Ref. 23. Furthermore, as a consequence of the different behaviors of conductance presented in Fig. 2(a), Fig. 3(a) also demonstrates that the oscillation of spin polarization in the GNRs with a large energy band gap is very strong in comparison with the others. For instance, the amplitude of P is about 65% for $M=21$ (semiconducting), while it is only few percent for $M=23$ (metallic) or has a maximum value of 30% in infinite graphene sheets.[22–24] However, since the energy band gap decreases, the oscillation of conductance and spin polarization weakens gradually when increasing the ribbon width. To illustrate this point, we display in Fig. 3(b) an example of the effect of different ribbon widths on the spin polarization in the semiconducting GNR structures ($M \neq 3n+2$). Indeed, when increasing the ribbon width, the amplitude of P decreases, i.e., it is only about 35% for $M=33$. In the limit of infinite width, the transport quantities in the GNRs tend to those in infinite graphene sheets [e.g., $|P| \sim 20\%$ as shown in Fig. 5(b) of Ref. 23], where continuum Dirac's description is valid.

B. Effects of normal-conducting leads

In this section, we consider the spin-dependent transport in the NGN junctions. Actually, the transport properties of this structure are essentially due to the difference in the dispersion relation in two materials. Our calculations show that a change in the ratio between the two lattice constants and in the value of t_L does not qualitatively affect the features observed. This is in agreement with Ref. 35. Moreover, to ensure that the interfaces are ballistic (without tunneling barriers) when $t_C=t$, the hopping energy t_L is chosen to be equal to t. First, we focus on the possibilities of obtaining high tunable spin-polarized current when replacing the graphitic leads by the normal-conducting ones. Second, we analyze the sensitivity of transport quantities to different parameters as the device length and the Fermi energy.

In Ref. 34, comparing resistances of NGN contacts with a zigzag interface and GGG ones, Schomerus found the duality between doped graphitic leads and quantum wires. It results in the same transport properties when the doping energies are suitably adjusted [i.e., Eq. (16) in Ref. 34]. The difference between two structures is only quantitative. On this basis, we display in Fig. 4(a) the conductance as a function of U_G in the NGN junction in comparison with the GGG structure for the case of a device length $L_D=51$ nm and a Fermi energy $E_F=300$ meV. Indeed, the obtained results are in good agreement with the conclusions in Ref. 34. Qualitatively, Fig. 4(a) shows that the oscillation of conductance seems to be unchanged in its phase and period when changing the leads. Quantitatively, the oscillation in the NGN junction is stronger than in the GGG structure. This can be explained clearly by the effect of replacing the graphitic leads by the normal-conducting ones on the picture of bound states in the barrier region. These states, in the framework of the Dirac's description, have been considered as confined hole states in graphene sheets.[23] In Fig. 4(b), we display the LDOS (see the right axis for graphitic and the left axis for normal-conducting leads) with respect to U_G at the first site of barrier region. The peaks of LDOS occur when the Fermi energy corresponds to any bound state. Obviously, the oscillation of LDOS (or the quantization of bound states in the barrier) in the NGN junction appears stronger (with higher

Author complimentary copy. Redistribution subject to AIP license or copyright, see http://jap.aip.org/jap/copyright.jsp

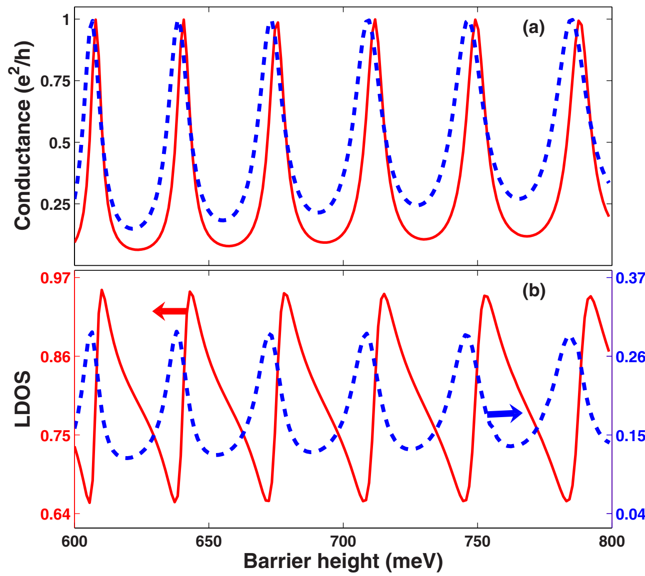

FIG. 4. (Color online) Comparison of conductance (a) and LDOS (b) in different structures: graphitic (dashed) and normal-conducting (solid lines, $t_C=t$) leads. Everywhere $M=21$, $L_D=51$ nm, $L_G=42.5$ nm, $E_F=300$ meV, and $h=0$ meV.

peaks) than in the GGG structure. It is the essential origin of the different behaviors of conductance, as shown in Fig. 4(a).

Now we turn to the behavior of spin-polarized current in ferromagnetic gate NGN junctions where $h=10$ meV. In Figs. 5(a) and 5(b), we show the comparison of spin polarization in the NGN junctions and in the GGG structures. Due to the different behaviors of conductance presented in Fig. 4(a), the amplitude of P in former structures is remarkably larger than in the latter ones. Particularly, when changing the leads, it increases from 65% to 81% [see Fig. 5(a)] and from 1% to 50% [see Fig. 5(b)] for $M=21$ and 23, respectively.

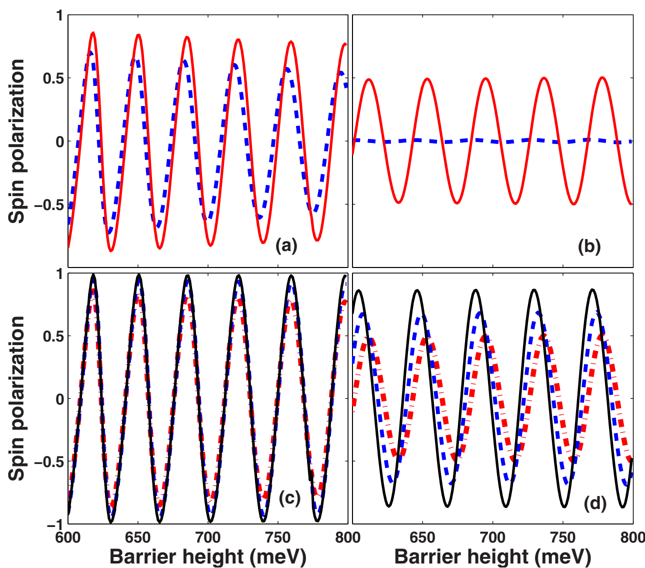

FIG. 5. (Color online) [(a) and (b)] Comparison of spin polarization in the different structures: graphitic (dashed) and normal-conducting (solid lines, $t_C=t$) leads. [(c) and (d)] The spin polarization in the latter one with different coupling strengths: $t_C=t$ (dashed), 0.8t (dashed-dotted), and 0.6t (solid lines). The ribbon widths are $M=21$ [(a) and (c)] and 23 [(b) and (d)]. Other parameters are $L_D=51$ nm, $L_G=42.5$ nm, $E_F=300$ meV, and $h=10$ meV.

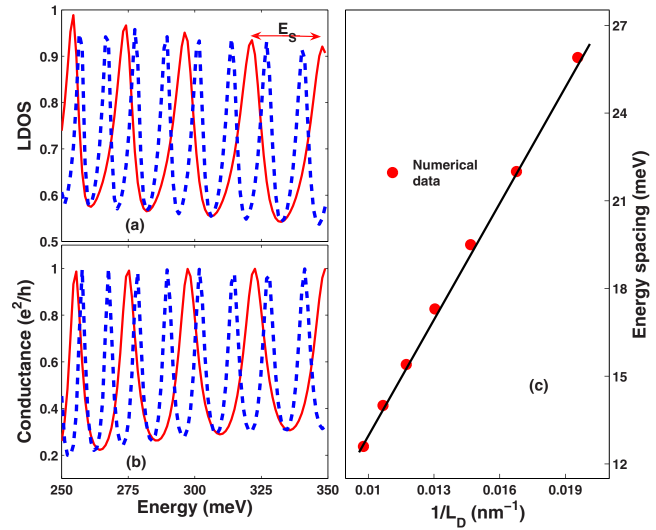

FIG. 6. (Color online) (a) LDOS illustrating the existence of confined states in the device and (b) conductance in the NGN junctions as a function of the Fermi energy for different device lengths: $L_D=51$ nm (solid) and 102 nm (dashed lines). (c) shows the dependence of energy spacing of confined states on the inverse of device length. Everywhere $M=21$, $L_G=42.5$ nm, $t_C=0.8t$, and $U_G=h=0$ meV.

Moreover, in the NGN junctions, the possibility of obtaining high tunable spin-polarized current is more impressive with decreasing the strength of device-to-contact coupling, which is characterized by the hopping energy t_C. In Figs. 5(c) and 5(d), we display the obtained results for three values of t_C: $t_C=t$ (dotted), 0.8t (dashed), and 0.6t (solid lines). Actually, the transport in the structure depends strongly on the properties of normal-conductor/graphene junctions and therefore on t_C. A smaller t_C corresponds to a higher contact resistance.[33] We find that the quantization of bound states in the barrier region is stronger when decreasing t_C (not shown), which leads to a stronger oscillation of the transport quantities with respect to the barrier height. Indeed, even in the case of $M=23$, the spin polarization can reach a very high value of 86% for $t_C=0.6t$ [see Fig. 5(d)]. More impressively, in the case of $M=21$, it can tend to 100% by reducing t_C [see Fig. 5(c)]. Some similar features such as giant magnetoresistance[29,30] and very high spin-polarized current[31] have been also observed in the GNR structures.

Practically, the features discussed above depend strongly on the parameters of the NGN junctions, such as the device length and/or the Fermi energy. It results from the fact that the charge transport can be confined in the device by two normal-conductor/graphene junctions. It leads to an additional resonant condition controlling the transport picture beside the transmission via the bound states in the barrier. Indeed, the existence of such confined states is demonstrated clearly from the behavior of LDOS shown in Fig. 6(a). In this figure, to cancel the effects of bound states in the barrier, the gate voltage is not applied to the device. The energy spacing E_S of confined states is then estimated to be about 25.4 meV for $L_D=51$ nm and 12.6 meV for 102 nm. In fact, E_S is inversely proportional to the device length, as illustrated in Fig. 6(c). This implies an unusual quantization of charges in the graphene-based structures, which is essentially different from the case of normal semiconductors wherein

Author complimentary copy. Redistribution subject to AIP license or copyright, see http://jap.aip.org/jap/copyright.jsp

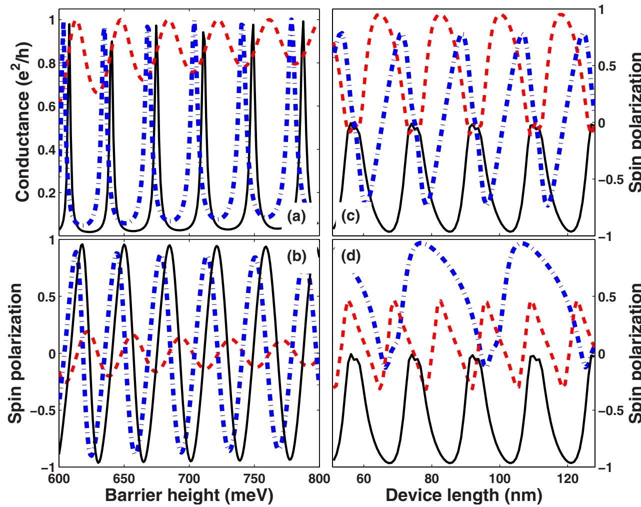

FIG. 7. (Color online) (a) Conductance and (b) spin polarization P in the NGN structures as functions of the barrier height U_G for different device lengths: 68 nm (solid), 74 nm (dashed), and 79 nm (dashed-dotted lines). The oscillation of P vs the device length for different values of U_G (c) [630 meV (solid), 655 meV (dashed-dotted), and 681 meV (dashed line)] and of E_F (d) [250 meV (dashed-dotted), 300 meV (solid), and 350 meV (dashed line)]. Other parameters are $M=21$, $L_G=42.5$ nm, $E_F=300$ meV [in (a)–(c)], $t_C=0.8t$, $U_G=630$ meV [in (d)] and $h=10$ meV.

$E_S \propto 1/L_D^2$ as previously discussed in Refs. 23 and 43. Due to such confinement, the transport quantities, such as the conductance and the spin polarization (not shown), have also an oscillatory behavior with respect to the Fermi energy in the considered region [see Fig. 6(b)]. Therefore, when a gate voltage is applied, there is a coexistence of bound states in the barrier and confined states in the device. They together respond for the resonant transport conditions of the structure.

On the other hand, the gate controllability of spin-polarized current is principally due to the picture of bound states in the barrier (or Klein's tunneling).[23] It arises a question about how the confined states in the device affect that picture. As shown in Figs. 4 and 5, the replacement of the graphitic leads (infinite L_D) by normal-conducting ones (finite L_D) does not affect the period but the amplitude of the oscillations. It suggests that, in the NGN junctions, the oscillation of conductance and spin polarization can be modulated in its amplitude while its period is unchanged when changing the device length. To examine this statement, we display the conductance in Fig. 7(a) and the spin polarization in Fig. 7(b) as a function of barrier height for different device lengths. From Fig. 7(a), we see that while the period ($U_P = v_g \pi / L_G$) is determined only by the gate length, the amplitude of conductance oscillation is modified when changing L_D, i.e., it is strong or weak when $L_D=68$ (and 79) or 74 nm, respectively. Consequently, the amplitude of spin polarization is dependent on L_D, i.e., it is about 95% for $L_D = 68$ nm, 15% for 74 nm, and 86% for 79 nm [see Fig. 7(b)]. This feature is exhibited more clearly in Fig. 7(c) by three curves of spin polarization versus L_D for different barrier heights: $U_G=630$ meV (dashed), 655 meV (dashed-dotted), and 681.5 meV (solid line). It is shown that P has an oscillatory behavior and is suppressed completely at certain values of L_D. Obviously, this demonstrates that the amplitude of spin polarization shown in Fig. 7(b) is also an oscillatory function of the device length. Moreover, its period seems to be inversely proportional to the Fermi energy, i.e., it is about 27.8 nm for $E_F=250$ meV, 18.3 nm for 300 meV, and 13.4 nm for 350 meV [see Fig. 7(d)]. It is nothing but a consequence of the resonant transport due to the confined states in the device. Hence, the gate control of spin-polarized current in the NGN junction can be modulated not only by the gate length L_G (discussed in the Sec. III A) but also by the device length L_D and/or the Fermi energy E_F. This implies that the structure should be carefully designed to obtain high controllability of spin-polarized current.

IV. CONCLUSIONS

Using the NEGF method for quantum transport simulation within the NNTB model, we have considered the spin-dependent transport in single ferromagnetic gate armchair GNRs. The leads are modeled as either graphitic or normal-conducting.

In the case of graphitic leads, it is shown that the conductance and the spin-polarized current behave as an oscillatory function of barrier height, which can be tuned by the gate voltage. The oscillation of spin polarization in the ribbon structures with a large energy band gap is strong in comparison with infinite graphene sheets. Especially, the study has demonstrated that a very high spin polarization can be observed in the NGN junctions. It is resulted from the fact that the quantization of bound states in the barrier (gated) region when using the normal-conducting leads may be stronger than in the case of graphitic ones. In these junctions, it is shown that the spin polarization increases and can tend to 100% by decreasing the strength of the device-to-contact coupling. Moreover, we have also found the existence of confined states in the device by normal-conductor/graphene junctions. This confinement responds for an additional resonant condition beside the transmission via the bound states in the barrier. As a result, the gate control of spin-polarized current in the NGN junctions can be modulated not only by the gate length but also by the device length and/or the Fermi energy.

Obtained results can be helpful for designing efficient spintronics devices based on the perfect armchair GNRs. However, some disorder effects, e.g., due to edge roughness, have been demonstrated experimentally[7] and may affect the transport properties[12] of the GNR structures. Further work is needed to assess their influence on the spin-polarized properties discussed in this article.

ACKNOWLEDGMENTS

This work was partially supported by the European Community through the Network of Excellence NANOSIL.

[1] A. H. Castro Neto, F. Guinea, N. M. R. Peres, K. S. Novoselov, and A. K. Geim, Rev. Mod. Phys. **81**, 109 (2009).
[2] K. S. Novoselov, A. K. Geim, S. V. Morozov, D. Jiang, Y. Zhang, S. V. Dubonos, I. V. Grigorieva, and A. A. Firsov, Science **306**, 666 (2004).
[3] K. S. Novoselov, A. K. Geim, S. V. Morozov, D. Jiang, M. I. Katsnelson, I. V. Grigorieva, S. V. Dubonos, and A. A. Firsov, Nature (London) **438**, 197 (2005).
[4] Y. Zhang, Y.-M. Tan, H. L. Stormer, and P. Kim, Nature (London) **438**, 201 (2005).

Author complimentary copy. Redistribution subject to AIP license or copyright, see http://jap.aip.org/jap/copyright.jsp

[5]N. Stander, B. Huard, and D. Goldhaber-Gordon, Phys. Rev. Lett. **102**, 026807 (2009).
[6]M. I. Katsnelson, K. S. Novoselov, and A. K. Geim, Nat. Phys. **2**, 620 (2006).
[7]M. Y. Han, B. Özyilmaz, Y. Zhang, and P. Kim, Phys. Rev. Lett. **98**, 206805 (2007); Z. Chen, Y.-M. Lin, M. J. Rooks, and P. Avouris, Physica E **40**, 228 (2007); X. Li, X. Wang, L. Zhang, S. Lee, and H. Dai, Science **319**, 1229 (2008).
[8]M. Fujita, K. Wakabayashi, K. Nakada, and K. Kasakabe, J. Phys. Soc. Jpn. **65**, 1920 (1996).
[9]K. Nakada, M. Fujita, G. Dresselhaus, and M. S. Dresselhaus, Phys. Rev. B **54**, 17954 (1996).
[10]Y. Kobayashi, K. Fukui, T. Enoki, and K. Kusakabe, Phys. Rev. B **73**, 125415 (2006).
[11]A. Cresti, N. Nemec, B. Biel, G. Niebler, F. Triozon, G. Cuniberti, and S. Roche, Nano Res. **1**, 361 (2008).
[12]D. Querlioz, Y. Apertet, A. Valentin, K. Huet, A. Bournel, S. Galdin-Retailleau, and P. Dollfus, Appl. Phys. Lett. **92**, 042108 (2008); A. Lherbier, B. Biel, Y.-M. Niquet, and S. Roche, Phys. Rev. Lett. **100**, 036803 (2008); M. Evaldsson, I. V. Zozoulenko, H. Xu, and T. Heinzel, Phys. Rev. B **78**, 161407(R) (2008).
[13]Y. Niimi, T. Matsui, H. Kambara, K. Tagami, M. Tsukada, and H. Fukuyama, Phys. Rev. B **73**, 085421 (2006).
[14]Recently, *ab initio* calculations demonstrated that there are no truly metallic GNRs. In other words, there always exists a gap (though very narrow) in the energy structure, regardless of ribbon width. It seems that the third nearest neighbor TB calculations reveal a similar result (see Ref. 11).
[15]C. L. Kane and E. J. Mele, Phys. Rev. Lett. **95**, 226801 (2005).
[16]C. Józsa, M. Popinciuc, N. Tombros, H. T. Jonkman, and B. J. van Wees, Phys. Rev. Lett. **100**, 236603 (2008).
[17]N. M. R. Peres, F. Guinea, and A. H. Castro Neto, Phys. Rev. B **72**, 174406 (2005).
[18]T. O. Wehling, K. S. Novoselov, S. V. Morozov, E. E. Vdovin, M. I. Katsnelson, A. K. Geim, and A. I. Lichtenstein, Nano Lett. **8**, 173 (2008).
[19]O. V. Yazyev and L. Helm, Phys. Rev. B **75**, 125408 (2007).
[20]Y.-W. Son, M. L. Cohen, and S. G. Louie, Nature (London) **444**, 347 (2006).
[21]H. Haugen, D. Huertas-Hernando, and A. Brataas, Phys. Rev. B **77**, 115406 (2008).
[22]T. Yokoyama, Phys. Rev. B **77**, 073413 (2008).
[23]V. Nam Do, V. Hung Nguyen, P. Dollfus, and A. Bournel, J. Appl. Phys. **104**, 063708 (2008).
[24]J. Zou, G. Jin, and Y.-Q. Ma, J. Phys.: Condens. Matter **21**, 126001 (2009).
[25]Y. G. Semenov, K. W. Kim, and J. M. Zavada, Appl. Phys. Lett. **91**, 153105 (2007).
[26]N. A. Sinitsyn, J. E. Hill, H. Min, J. Sinova, and A. H. MacDonald, Phys. Rev. Lett. **97**, 106804 (2006).
[27]S. Cho, Y.-F. Chen, and M. S. Fuhrer, Appl. Phys. Lett. **91**, 123105 (2007).
[28]L. Brey and H. A. Fertig, Phys. Rev. B **76**, 205435 (2007).
[29]A. Saffarzadeh and M. Ghorbani Asl, Eur. Phys. J. B **67**, 239 (2009).
[30]F. Munoz-Rojas, J. Fernandez-Rossier, and J. J. Palacios, Phys. Rev. Lett. **102**, 136810 (2009).
[31]H. Sahin and R. T. Senger, Phys. Rev. B **78**, 205423 (2008).
[32]B. Huard, J. A. Sulpizio, N. Stander, K. Todd, B. Yang, and D. Goldhaber-Gordon, Phys. Rev. Lett. **98**, 236803 (2007).
[33]M. Ya. Blanter and I. Martin, Phys. Rev. B **76**, 155433 (2007).
[34]H. Schomerus, Phys. Rev. B **76**, 045433 (2007).
[35]J. P. Robinson and H. Schomerus, Phys. Rev. B **76**, 115430 (2007).
[36]M. P. Lopez Sancho, J. M. Lopez Sancho, and J. Rubio, J. Phys. F: Met. Phys. **14**, 1205 (1984).
[37]M. P. Anantram, M. S. Lundstrom, and D. E. Nikonov, Proc. IEEE **96**, 1511 (2008).
[38]Y. Imry and R. Landauer, Rev. Mod. Phys. **71**, S306 (1999).
[39]L. Chico, V. H. Crespi, L. X. Benedict, S. G. Louie, and M. L. Cohen, Phys. Rev. Lett. **76**, 971 (1996).
[40]Y. Klymenko, L. Malysheva, and A. Onipko, Phys. Status Solidi B **245**, 2181 (2008).
[41]C. Tang, Y. Zheng, G. Li, and L. Li, Solid State Commun. **148**, 455 (2008).
[42]E. W. Hill, A. K. Geim, K. Novoselov, F. Schedin, and P. Blake, IEEE Trans. Magn. **42**, 2694 (2006).
[43]J. M. Pereira, Jr., V. Mlinar, F. M. Peeters, and P. Vasilopoulos, Phys. Rev. B **74**, 045424 (2006).

Author complimentary copy. Redistribution subject to AIP license or copyright, see http://jap.aip.org/jap/copyright.jsp